



**HAL**  
open science

## Piezoelectric and mechanical behavior of NaNbO<sub>3</sub>/PEKK lead-free nanocomposites

Camille Bessaguet, Eric Dantras, Colette Lacabanne, Mathieu Chevalier,  
Guilhem Michon

► **To cite this version:**

Camille Bessaguet, Eric Dantras, Colette Lacabanne, Mathieu Chevalier, Guilhem Michon. Piezoelectric and mechanical behavior of NaNbO<sub>3</sub>/PEKK lead-free nanocomposites. *Journal of Non-Crystalline Solids*, 2017, 459, pp.83-87. 10.1016/j.jnoncrysol.2016.12.030 . hal-01481093

**HAL Id: hal-01481093**

**<https://hal.science/hal-01481093>**

Submitted on 8 Mar 2017

**HAL** is a multi-disciplinary open access archive for the deposit and dissemination of scientific research documents, whether they are published or not. The documents may come from teaching and research institutions in France or abroad, or from public or private research centers.

L'archive ouverte pluridisciplinaire **HAL**, est destinée au dépôt et à la diffusion de documents scientifiques de niveau recherche, publiés ou non, émanant des établissements d'enseignement et de recherche français ou étrangers, des laboratoires publics ou privés.



## Open Archive TOULOUSE Archive Ouverte (OATAO)

OATAO is an open access repository that collects the work of Toulouse researchers and makes it freely available over the web where possible.

This is an author-deposited version published in : <http://oatao.univ-toulouse.fr/>  
Eprints ID : 17434

**To link to this article** : DOI : 10.1016/j.jnoncrysol.2016.12.030  
URL : <http://dx.doi.org/10.1016/j.jnoncrysol.2016.12.030>

**To cite this version** : Bessaguet, Camille and Dantras, Eric and Lacabanne, Colette and Chevalier, Mathieu and Michon, Guilhem *Piezoelectric and mechanical behavior of NaNbO<sub>3</sub>/PEKK lead-free nanocomposites*. (2017) Journal of Non-Crystalline Solids, vol. 459. pp. 83-87. ISSN 0022-3093

Any correspondence concerning this service should be sent to the repository administrator: [staff-oatao@listes-diff.inp-toulouse.fr](mailto:staff-oatao@listes-diff.inp-toulouse.fr)

# Piezoelectric and mechanical behavior of $\text{NaNbO}_3/\text{PEKK}$ lead-free nanocomposites

C. Bessaguet<sup>a,b,c</sup>, E. Dantras<sup>b,\*</sup>, C. Lacabanne<sup>b</sup>, M. Chevalier<sup>a</sup>, G. Michon<sup>c</sup>

<sup>a</sup> Institut de Recherche Technologique (IRT) Saint Exupéry, 118 route de Narbonne, CS 44248, 31432, Toulouse cedex 4, France

<sup>b</sup> Physique des Polymères, Institut Carnot CIRIMAT, Université Paul Sabatier, 118 route de Narbonne, 31062, Toulouse cedex 09, France

<sup>c</sup> Institut Supérieur de l'Aéronautique et de l'espace, Institut Clément Ader, 3 rue Caroline Aigle, 31400 Toulouse, France

## A B S T R A C T

Lead-free piezoelectric nanocomposites based on poly(ether ketone ketone) (PEKK) and sodium niobate ( $\text{NaNbO}_3$ ) particles were elaborated. The presence of submicronic particles does not influence the thermal stability of the matrix so that no degradation phenomenon is observed before 500 °C. The conservative mechanical modulus  $G'$  increases linearly with the  $\text{NaNbO}_3$  fraction; this variation is well fitted by the Kerner model until 20 vol%. Such nanocomposites remain ductile. The polarizing field required for obtaining piezoelectric nanocomposites is  $12 \text{ kV} \cdot \text{mm}^{-1}$  i.e. analogous with the one used for poling bulk ceramic. The value of the piezoelectric coefficient ( $d_{33} = 0.2 \text{ pC} \cdot \text{N}^{-1}$  for 20 vol%  $\text{NaNbO}_3$ ) is consistent with the Furukawa's model. This value is explained by the low PEKK permittivity. This low  $d_{33}$  is counterbalanced by the piezoelectric voltage constant ( $g_{33} = 103 \cdot 10^{-3} \text{ Vm} \cdot \text{N}^{-1}$ ) which is higher than the one of classical piezoelectric ceramic like PZT or  $\text{BaTiO}_3$ .

## Keywords:

Lead-free ceramic  
Piezoelectric nanocomposite  
Poly(ether ketone ketone)  
Sodium niobate  
Dynamic mechanical analysis  
Permittivity

## 1. Introduction

The first extrinsic piezoelectric composite has been elaborated in 1976 by Furukawa. Micronic electroactive particles of lead zirconate titanate (PZT) have been dispersed in a polyepoxy matrix [1]. This kind of particles has been widely used subsequently, especially for applications of sensors and actuators due to a high Curie temperature and a high piezoelectric coefficient [2–6]. However, the recent legislation about lead toxicity [7] has highly stimulated the use of lead-free ceramic such as barium titanate ( $\text{BaTiO}_3$ ) [8–12], potassium niobate ( $\text{KNbO}_3$ ) [13–15], lithium niobate ( $\text{LiNbO}_3$ ) [16,17], and sodium niobate ( $\text{NaNbO}_3$ ) [13, 18–20].

The interest of this study is the integration of the piezoelectric property using a lead-free piezoelectric ceramic in a structural polymer for aeronautical and space applications. Carponcin et al. [5] have studied the integration of PZT in poly(ether ether ketone) (PEEK). They showed that it was possible to disperse homogeneously electroactive particles in a high-performance thermoplastic matrix to bring it piezoelectric property. In this paper, the host matrix is the poly(ether ketone ketone) (PEKK), a high performance thermoplastic polymer also belonging to the poly(aryl ether ketone) (PAEK) family. PEKK has a melting temperature lower than PEEK making it less expensive for industrial processing. The lead-free selected electroactive ceramic was the  $\text{NaNbO}_3$ . It

has a high Curie temperature ( $T_c$ ) compatible with the matrix [21–23] and an interesting bulk piezoelectric coefficient ( $d_{33}$ ) [24,25]. The main challenge in piezoelectric composite processing is the polarization step. It is a critical step which is essential to obtain a piezoelectric material. It consists in applying an electric field (higher than the coercive field of the piezoelectric element) through the sample in order to orient the electric dipoles. Another advantage of  $\text{NaNbO}_3$  is its low coercive field [26] and therefore it requires a low polarization field that limits the risk of breakdowns [27].

The present paper describes the synthesis and the characterization of  $\text{NaNbO}_3$ . Then, the elaboration and polarization protocol are presented. We will focus on the influence of  $\text{NaNbO}_3$  particles on thermal stability, mechanical and electroactive properties of  $\text{PEKK}/\text{NaNbO}_3$  nanocomposites.

## 2. Materials and methods

### 2.1. $\text{NaNbO}_3$ submicronic particles elaboration

$\text{NaNbO}_3$  particles were synthesized for the first time by Goh et al. [13] in 2003 using a hydrothermal synthesis. The structural evolution of  $\text{NaNbO}_3$  during the reaction was studied more precisely by Zhu et al. [18]. First, fine powders aggregate to form irregular bars that grow into nanowires and finally submicronic particles. In this work, the David et al. [27] protocol, based on Goh's one, has been used. Niobium pentoxide ( $\text{Nb}_2\text{O}_5$ ) and concentrated sodium hydroxide (10 M)

\* Corresponding author.

E-mail address: eric.dantras@univ-tlse3.fr (E. Dantras).

were mixed in an autoclave and heated above 150 °C. The white compound obtained ( $\text{Na}_2\text{Nb}_2\text{O}_6 \cdot 2/3\text{H}_2\text{O}$ ) was filtered out, washed with de-ionized water and dried in an oven at 100 °C.  $\text{NaNbO}_3$  particles were obtained after an annealing at 600 °C for 6 h.

## 2.2. PEKK/ $\text{NaNbO}_3$ nanocomposite elaboration process

Ceramic particles were milled with a mortar in order to break any aggregates. They were dispersed in ethanol with ultrasound and mixed with the polymer powder. After ethanol evaporation, the PEKK/ $\text{NaNbO}_3$  nanocomposite powder was homogeneous. PEKK/ $\text{NaNbO}_3$  mix was processed using a twin screw extruder at 360 °C during 15 min at 30 rpm. Nanocomposites with different volume fractions were elaborated from 3% to 30% in volume fraction.

Fig. 1 represents a scanning electron microscopy (SEM) micro cut of PEKK/ $\text{NaNbO}_3$  20 vol% sample. Particle dispersion in the polymer matrix was homogeneous at this scale. Dispersion quality is an important parameter to facilitate the polarization process and prevent from electrical breakdowns.

## 2.3. Polarization process

The polarization process consists in orienting electric dipoles to obtain a macroscopic piezoelectric effect [10]. The material was inserted under a high static electric field at a given isotherm. During the cooling, the electric field was maintained in order to fix the dipole orientation. Polarization temperature, electric field value and poling time were optimized.

The following Eq. (1) makes the link between the field really seen by the particles  $\vec{E}_p$ , the matrix and particle permittivities,  $\epsilon_M$  and  $\epsilon_p$  respectively, and the applied electric field  $\vec{E}_{appl}$  [8].

$$\vec{E}_p = \frac{3\epsilon_M}{\epsilon_p + 2\epsilon_M} \vec{E}_{appl} = L_E \vec{E}_{appl} \quad (1)$$

To optimize  $\vec{E}_p$  (and therefore the polarization efficiency), the ratio between matrix and particle permittivity is crucial. A dynamic dielectric analysis was performed on the PEKK in order to determine the evolution of the matrix permittivity as a function of temperature. Above the dielectric manifestation of the glass transition ( $T_\alpha$ ),  $\epsilon_M$  increases; it is suitable for the polarization. Thus, the polarization was performed at a temperature higher than  $T_\alpha$  ( $T_{pol} \approx 180$  °C) under an electric field higher than the coercive field ( $E_{pol} \approx 12 \text{ kV} \cdot \text{mm}^{-1}$ ) during 15 min. To avoid

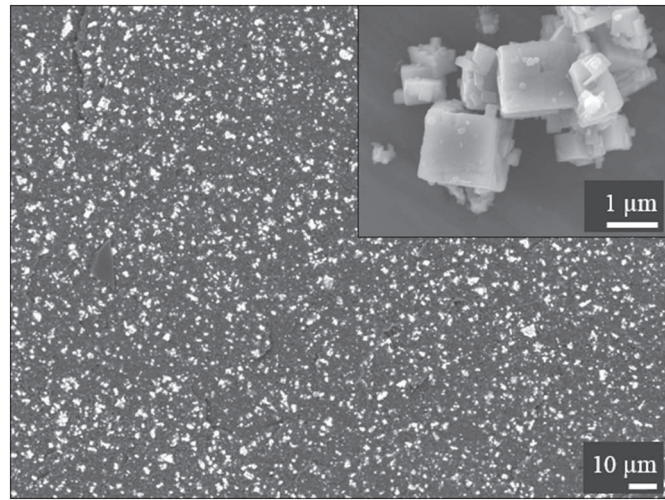


Fig. 1. SEM image of PEKK/ $\text{NaNbO}_3$  micro cut with a volume fraction of 20% (scale bar: 10  $\mu\text{m}$ ). In the insert:  $\text{NaNbO}_3$  particles (scale bar: 1  $\mu\text{m}$ ).

breakdowns and to optimize the isotherm quality, samples were immersed in an oil bath. After the polarization process, nanocomposites were short-circuited during 24 h and the piezoelectric coefficient ( $d_{33}$ ) was measured.

## 3. Experimental

Thermogravimetric analysis (TGA Q50 from TA instruments with an accuracy of  $\pm 1$  wt%) was performed under air atmosphere at  $20$  °C  $\cdot$  min $^{-1}$  to measure the nanocomposites thermal stability and determine the experimental volume fraction of sodium niobate. The physical structure, as the glass transition, the crystallinity rate and the melting temperatures, was determined by differential scanning calorimetry (DSC) using a DSC7 from Perkin Elmer with a temperature accuracy of  $\pm 0.1$  °C and an enthalpy accuracy of  $\pm 0.2$  J  $\cdot$  g $^{-1}$ . The crystallinity rate was determined by normalizing the matrix fraction. To study nanocomposites mechanical properties, dynamical mechanical analysis (DMA, ARES) was performed in rectangular mode. The applied deformation and angular frequency were fixed at 0.1% and 1 rad  $\cdot$  s $^{-1}$  respectively. The particle morphology and the particle dispersion quality were observed using a scanning electron microscope (MEB-FEG JEOL JSM 7800F Prime) using secondary and backscattered electron detection. After the nanocomposites polarization (see “polarization process” section), the piezoelectric coefficient ( $d_{33}$ ) was measured using a Piezometer system from Piezotest with frequency and force of 110 Hz and 0.25 N respectively.

## 4. Results

### 4.1. $\text{NaNbO}_3$ analysis

Inset of Fig. 1 represents SEM image of  $\text{NaNbO}_3$  particles. They were cubic with a low aspect ratio. The particle size was about 1  $\mu\text{m}$ . Due to a high Curie temperature ( $T_c$ ) and a weak modification of crystalline lattice parameters, conventional techniques as DSC or x-ray diffraction (DRX) could not be used to determine  $T_c$ . A non-classical protocol has been developed: A ceramic disk was manufactured by spark plasma sintering (SPS) to limit the grain growth, polarized under a static field and annealed at different temperatures until Curie transition. The maximum  $d_{33}$  was measured at  $34.5 \text{ pC} \cdot \text{N}^{-1}$  which is coherent with the literature [25,28].

Fig. 2 represents the  $d_{33}$  evolution as a function of annealing temperature.  $T_c$  was measured at 287 °C.

### 4.2. Thermal stability

Fig. 3 shows the weight loss as a function of temperature for nanocomposites with different  $\text{NaNbO}_3$  volume fraction. Under air

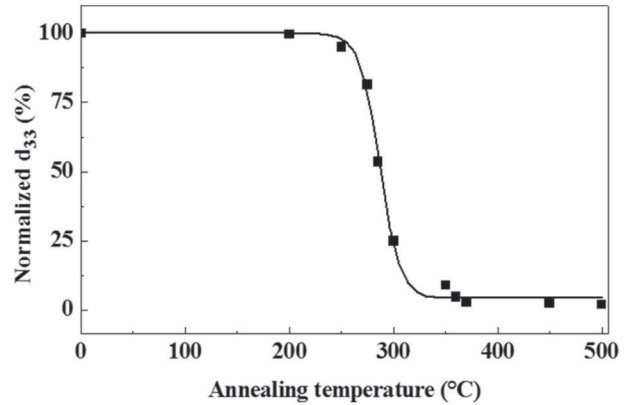
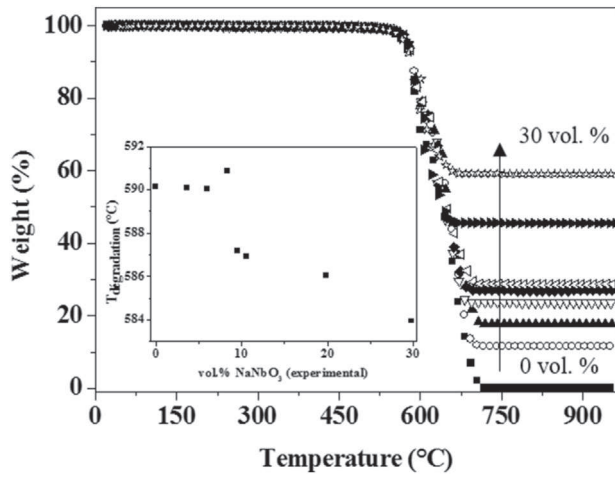


Fig. 2.  $d_{33}$  evolution of  $\text{NaNbO}_3$  disk versus annealing temperature. The line is drawn as a guide to the eyes.



**Fig. 3.** TGA thermogram of PEKK and PEKK/NaNbO<sub>3</sub>: (■) PEKK, (○) PEKK/NaNbO<sub>3</sub> 4 vol%, (▲) PEKK/NaNbO<sub>3</sub> 6 vol%, (▽) PEKK/NaNbO<sub>3</sub> 9 vol%, (◆) PEKK/NaNbO<sub>3</sub> 10 vol%, (◁) PEKK/NaNbO<sub>3</sub> 11 vol%, (►) PEKK/NaNbO<sub>3</sub> 20 vol%, (★) PEKK/NaNbO<sub>3</sub> 30 vol%. In the inset: evolution of the degradation temperature versus the experimental vol% of NaNbO<sub>3</sub>.

atmosphere, above 750 °C, PEKK was totally degraded. The weight residue corresponds directly to the weight fraction of particles. The experimental volume fraction of NaNbO<sub>3</sub> is calculated from the residue at 900 °C. The degradation temperature ( $T_d$ ) is measured at the peak maximum of the weight loss derivate curve. Inset of Fig. 3 represents the evolution of  $T_d$  as a function of NaNbO<sub>3</sub> volume fraction. Until 6 vol%,  $T_d$  is stable. It appears that for higher fractions,  $T_d$  decreases when the fraction of NaNbO<sub>3</sub> increases.

#### 4.3. Physical structure

Nanocomposites physical structure has been studied. Fig. 4 shows the evolution of the melting temperature and crystallinity ratio as a function of NaNbO<sub>3</sub> volume fraction.

The melting temperature and the crystallinity ratio decrease linearly. Particles do not promote crystallinity and reduce the cohesion of the crystal. In addition, presence of particles does not change the glass transition temperature which means that NaNbO<sub>3</sub> particles do not affect the chain mobility or the free volume of the amorphous phase.

#### 4.4. Mechanical properties

Fig. 5 shows the evolution of conservative  $G'$  and dissipative  $G''$  modulus of the neat PEKK over a wide range of temperature.  $G''$  highlights 3 relaxation modes [29,30]:  $\alpha$  mode at 165 °C is associated with the

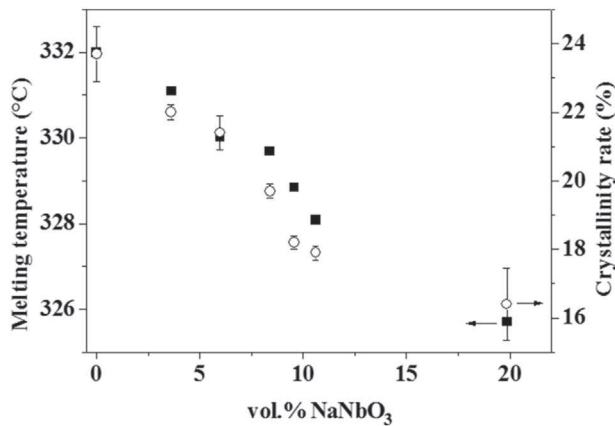


**Fig. 4.** Melting temperature (■) and crystallinity ratio (○) versus NaNbO<sub>3</sub> vol% for PEKK/NaNbO<sub>3</sub> nanocomposites during the 2nd run.

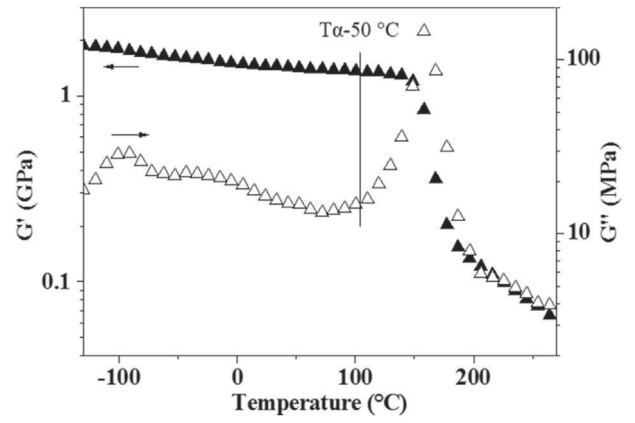


**Fig. 5.** Evolution of the conservative  $G'$  (▲) and dissipative  $G''$  (△) modulus of PEKK versus temperature.

mechanical manifestation of the glass transition,  $\beta$  mode between  $-60$  °C and  $0$  °C, with the oscillation of the aromatic rings around the main chain and finally, the localized  $\gamma$  mode between  $-130$  °C and  $-60$  °C highlights the interaction between ketone functions and absorbed water.

The evolution of the vitreous modulus of PEKK/NaNbO<sub>3</sub> nanocomposites is presented in Fig. 6 as a function of temperature for different volume fraction of NaNbO<sub>3</sub>. The value of the vitreous plateau increases with the introduction of NaNbO<sub>3</sub>, from 1.5 GPa to 3.7 GPa at 20 °C. Inset of Fig. 6 represents  $G'$  measured at  $T_{\alpha}-50$  °C as a function of NaNbO<sub>3</sub> volume fraction.

It increases linearly until 20 vol%. To explain the critical increase of  $G'$  for the last nanocomposite experimental data were fitted with the Kerner model (solid line). It is based on the hypothesis that spherical particles (or particles with a low aspect ratio) without interaction, are randomly dispersed in the matrix. Nanocomposite conservative modulus is given by the Eq. (2) [31]:

$$G_c = G_m \left( \frac{\frac{\phi G_p}{(7-5v_m)G_m + (8-10v_m)G_p} + \frac{(1-\phi)}{15(1-v_m)}}{\frac{\phi G_m}{(7-5v_m)G_m + (8-10v_m)G_p} + \frac{(1-\phi)}{15(1-v_m)}} \right) \quad (2)$$

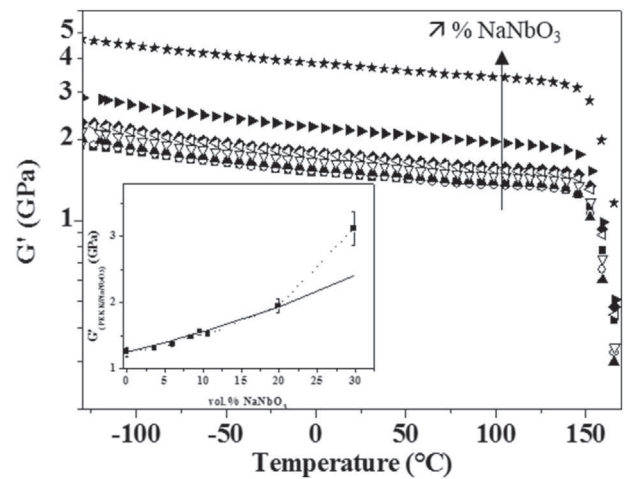


**Fig. 6.** Real part of the shear modulus (■) versus temperature of PEKK and PEKK/NaNbO<sub>3</sub>: (■) PEKK, (○) PEKK/NaNbO<sub>3</sub> 4 vol%, (▲) PEKK/NaNbO<sub>3</sub> 6 vol%, (▽) PEKK/NaNbO<sub>3</sub> 9 vol%, (◆) PEKK/NaNbO<sub>3</sub> 10 vol%, (◁) PEKK/NaNbO<sub>3</sub> 11 vol%, (►) PEKK/NaNbO<sub>3</sub> 20 vol%, (★) PEKK/NaNbO<sub>3</sub> 30 vol%. In the inset: value of the vitreous plateau measured at  $T_{\alpha}-50$  °C versus vol%. The solid line represents the fit of experimental data with the Kerner model.

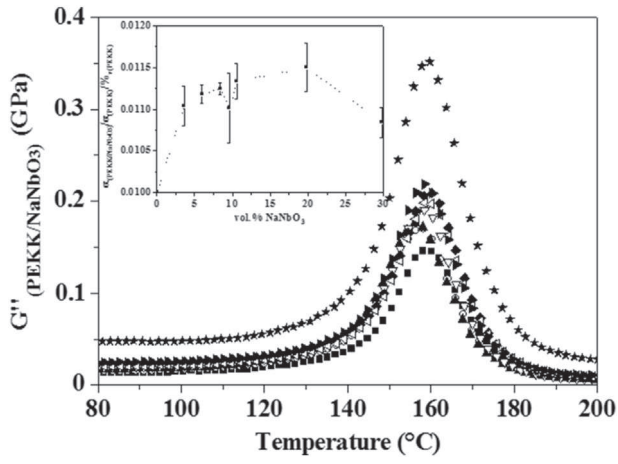


Fig. 7. Imaginary part of the shear modulus (■) versus temperature of PEKK and PEKK/NaNbO<sub>3</sub>: (■) PEKK, (○) PEKK/NaNbO<sub>3</sub> 4 vol%, (▲) PEKK/NaNbO<sub>3</sub> 6 vol%, (▽) PEKK/NaNbO<sub>3</sub> 9 vol%, (◆) PEKK/NaNbO<sub>3</sub> 10 vol%, (◁) PEKK/NaNbO<sub>3</sub> 11 vol%, (▶) PEKK/NaNbO<sub>3</sub> 20 vol%, (★) PEKK/NaNbO<sub>3</sub> 30 vol%. In the inset: specific energy loss normalized by the matrix fraction versus vol%.

where  $G_c$ ,  $G_m$  and  $G_p$  are respectively the shear modulus of nanocomposites, matrix and particles,  $\nu_m$  is the Poisson coefficient and  $\phi$  is the volume fraction of particles.

Until 20 vol% experimental data are fitted well with this model. Thus, hypotheses are verified. For the nanocomposite with 30 vol% of NaNbO<sub>3</sub>, the experimental mechanical values depart from the model prediction.

The evolution of the dissipative modulus  $G''$  of PEKK/NaNbO<sub>3</sub> nanocomposites as a function of temperature related to the  $\alpha$  mode is presented in Fig. 7 for different volume fraction of NaNbO<sub>3</sub>. The area under the curve (noted as  $\alpha_{PEKK}$  and  $\alpha_{PEKK/NaNbO_3}$  for PEKK and its nanocomposites respectively) represents the energy dissipated by the polymer matrix due to the viscoelastic relaxation. Inset of Fig. 7 represents the specific energy loss normalized by the matrix fraction as a function of NaNbO<sub>3</sub> volume fraction. Presence of ceramic particles leads to an increase of the dissipated energy. The same shift is observed for  $\beta$  and  $\gamma$  modes at the same temperatures.

#### 4.5. Piezoelectric properties

$d_{33}$  coefficient of nanocomposites was measured 24 h after the polarization step. Fig. 8 a) represents the evolution of  $d_{33}$  as a function of NaNbO<sub>3</sub> volume fraction. Experimental data were fitted with the Furukawa's model [2] (solid line in Fig. 8 a) according to the following Eq. (3):

$$d_{33} = \phi L_E d_{33incl} \quad (3)$$

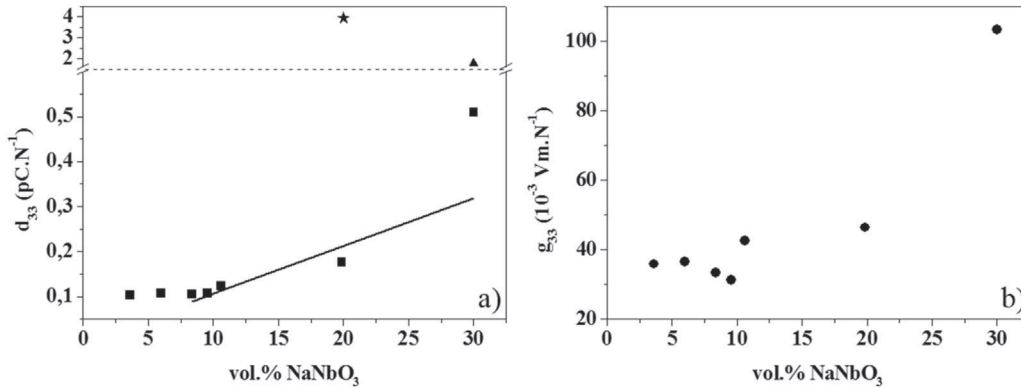


Fig. 8. Evolution of the piezoelectric coefficient  $d_{33}$  (■) fitted with the Furukawa's model (solid line) a) and the piezoelectric voltage constant  $g_{33}$  (●) b) of PEKK/NaNbO<sub>3</sub> versus NaNbO<sub>3</sub> vol%. (★) corresponds to PVDF/NaNbO<sub>3</sub> and (▲) PZT/PEEK nanocomposites [5].

where  $d_{33}$  is the piezoelectric coefficient of nanocomposites,  $\phi$  the volume fraction of NaNbO<sub>3</sub>,  $L_E$  the local field applied [8] and  $d_{33incl}$  the intrinsic piezoelectric coefficient of bulk NaNbO<sub>3</sub>.

This model considers a 2-phases system composed of a non-piezoelectric continuous phase where piezoelectric particles are randomly dispersed.

From 8 vol%, the variation of  $d_{33}$  is quasi-linear and experimental data are closed to the expected values. Particles are well dispersed into the matrix until 20 vol%.

In addition to the  $d_{33}$ , the piezoelectric voltage constant  $g_{33}$  is another piezoelectric parameter given by the following Eq. (4) [27]:

$$g_{33} = \frac{d_{33}}{\epsilon_M} \quad (4)$$

For bulk piezoelectric ceramic,  $d_{33}$  and  $\epsilon_M$  are both high. For organic polymer where piezoelectric ceramics are dispersed,  $d_{33}$  is low. But it is counterbalanced by a very low matrix permittivity. Fig. 8 b) shows the evolution of  $g_{33}$  with the NaNbO<sub>3</sub> volume fraction. The low matrix permittivity leads to a high value of  $g_{33}$  ( $g_{33}(\text{PEKK}/30 \text{ vol\% NaNbO}_3 = 104 \cdot 10^{-3} \text{ Vm} \cdot \text{N}^{-1}$ ).

## 5. Discussion

### 5.1. Curie temperature measurement

Literature reports values from 180 °C to 370 °C for the  $T_c$  of NaNbO<sub>3</sub>. The discrepancy obtained could be explained by poly crystallinity and/or particle size. Most of the time,  $T_c$  measurements were performed on mono crystals [21]. Hydrothermal synthesis tends to promote poly crystals. Furthermore, Moure et al. [22] show the influence of particle size on  $T_c$ . Particles with size higher than 1  $\mu\text{m}$  have a  $T_c$  at 370 °C. For particles with a size between 200 and 400 nm,  $T_c$  ranges from 310 °C to 330 °C and finally for particle size lower than 70 nm,  $T_c$  is measured at 180 °C. In this work, a size distribution probably exists and could explain the low value of  $T_c$ .

### 5.2. Conservative and dissipative modulus

For the nanocomposite with 30 vol% of NaNbO<sub>3</sub>, experimental data of conservative modulus depart from the model prediction (Kerner model). This is due to a change of the composite connectivity from 0–3 to 3–3 [32] that probably suppose a contact between particles and therefore critical modifications of the mechanical properties.

The increase of the dissipated energy (calculated from the area under the dissipative modulus) with the introduction of particles could be due to a friction phenomenon called “stick slip” at the interface between stiff particles and soft matrix [33]. In addition, it is interesting

to note that mode temperatures are not modified by the introduction of  $\text{NaNbO}_3$ , so the molecular mobility is unchanged by the presence of particles.

### 5.3. Piezoelectric coefficients

For the PEKK/ $\text{NaNbO}_3$  30 vol%, experimental data diverge from the Furukawa model. The change of connectivity also affects the piezoelectric property. However, the  $d_{33}$  values obtained are low. Particle and matrix permittivities have a strong influence on the polarization efficiency. On the one hand, a PVDF/20 vol%  $\text{NaNbO}_3$  nanocomposites was elaborated with the same process and polarized. Its  $d_{33}$  is higher ( $3.95 \text{ pC}\cdot\text{N}^{-1}$ ) (see Fig. 8 a) due to the higher permittivity of the PVDF (12 for PVDF, 2.7 for PEKK at RT). This value is coherent with the  $d_{33}$  value predicted by Furukawa's theoretical model. On the other hand, the influence of the particle intrinsic  $d_{33}$  is important. To give an example PEEK/PZT 30 vol% nanocomposite has a  $d_{33}$  of  $1.95 \text{ pC}\cdot\text{N}^{-1}$  [5] due to a high  $d_{33}$  of PZT ( $240 \text{ pC}\cdot\text{N}^{-1}$ ) [34].

Nevertheless,  $g_{33}$  (PEKK/30 vol%  $\text{NaNbO}_3$ ) is higher than common piezoelectric ceramics like  $\text{BaTiO}_3$  ( $g_{33}(\text{BaTiO}_3) = 11 \cdot 10^{-3} \text{ Vm}\cdot\text{N}^{-1}$ ) or PZT ( $g_{33}(\text{PZT}) = 52 \cdot 10^{-3} \text{ Vm}\cdot\text{N}^{-1}$ ).

## 6. Conclusion

Piezoelectric nanocomposites were elaborated using a high performance thermostable thermoplastic polymer and a lead-free piezoelectric ceramic. Submicronic  $\text{NaNbO}_3$  was synthesized via a hydrothermal synthesis. The dispersion process leads to a good dispersion of particles in the PEKK. Particles do not influence the thermal stability of matrix: no degradation is observed before  $500^\circ\text{C}$ . Melting temperature and crystallinity rate decrease with the  $\text{NaNbO}_3$  volume fraction. As for mechanical properties, the value of the vitreous plateau generates an increase of the nanocomposite rigidity. We observe a stick-slip phenomenon that increases the dissipated energy related to the viscoelastic relaxation when the particle fraction increases. Polarization is a critical step due to high temperature and high electric field required. The piezoelectric coefficient increases with the ceramic particles content but remains low due to low matrix permittivity. For other applications, the  $d_{33}$  could be improved with matrix of higher permittivity. It is important to note that the piezoelectric voltage constant  $g_{33}$  is higher than for common inorganic piezoelectric ceramic like PZT or  $\text{BaTiO}_3$ .

## Acknowledgments

These results were obtained under the research project "COMPINNOVTP" at the IRT Saint Exupéry. We thank the industrial and academic members of the IRT who supported this project through their contributions, both financial and in terms of specific knowledge:

- Industrial members: AIRBUS OPERATIONS, AIRBUS DEFENCE & SPACE, AIRBUS HELICOPTERS, AIRBUS GROUP INNOVATIONS and THALES ALENIA SPACE
- Academic members: CIRIMAT, ISAE, ICA, IMRCP, UPS and CNRS

We also thank the Commissariat Général aux Investissements and the Agence Nationale de la Recherche for their financial support in the Programme d'Investissement d'Avenir (PIA).

## References

- [1] T. Furukawa, K. Fujino, E. Fukada, Electromechanical properties in the composites of epoxy resin and PZT ceramics, *Jpn. J. Appl. Phys.* 15 (1976) 2119–2129.
- [2] T. Furukawa, K. Ishida, E. Fukada, T. Furukawa, K. Ishida, E. Fukada, Piezoelectric properties in the composite systems of polymers and PZT ceramics, *J. Appl. Phys.* 50 (1979) 4904–4912.
- [3] A. Jain, K.J. Prashanth, A.K. Sharma, A. Jain, P.N. Rashmi, Dielectric and piezoelectric properties of PVDF/PZT composites: a review, *Polym. Eng. Sci.* (2015) 1589–1616.
- [4] V. Tiwari, G. Srivastava, Structural, dielectric and piezoelectric properties of 0–3 PZT/PVDF composites, *Ceram. Int.* 41 (2015) 8008–8013.
- [5] D. Carponcin, E. Dantras, L. Laffont, J. Dandurand, G. Aridon, F. Levallois, L. Cadiergues, C. Lacabanne, Integrated piezoelectric function in a high thermostable thermoplastic PZT/PEEK composite, *J. Non-Cryst. Solids* 388 (2014) 32–36.
- [6] S. Touhtouh, M. Rguiti, C. Courtois, F. Belhora, A. Arbaoui, S. Dastorg, A. Rachek, A. Hajjaji, PU/PZT composites for vibratory energy harvesting, *Opt. Quant. Electron.* 48 (2016) 246.
- [7] Directive 2002/95/EC of the European Parliament and of the Council of the European Union, *Off. J. Eur. Union* 37 (2003) 19–51.
- [8] H.L.W. Chan, M.C. Cheung, C.L. Choy, Study on  $\text{BaTiO}_3/\text{P}(\text{VDF-TrFE})$  0-3 composites, *Ferroelectrics* 224 (1999) 113–120.
- [9] J. Yuh, J.C. Nino, W.M. Sigmund, Synthesis of barium titanate ( $\text{BaTiO}_3$ ) nanofibers via electrospinning, *Mater. Lett.* 59 (2005) 3645–3647.
- [10] J.F. Capsal, E. Dantras, L. Laffont, J. Dandurand, C. Lacabanne, Nanotexture influence of  $\text{BaTiO}_3$  particles on piezoelectric behaviour of PA 11/ $\text{BaTiO}_3$  nanocomposites, *J. Non-Cryst. Solids* 356 (2010) 629–634.
- [11] M.D. Toomey, K. Gao, G.P. Mendis, E.B. Slamovich, J.A. Howarter, Hydrothermal synthesis and processing of barium titanate nanoparticles embedded in polymer films, *ACS Appl. Mater. Interfaces* 7 (2015) 28640–28646.
- [12] S. Dalle Vacche, Y. Leterrier, V. Michaud, D. Damjanovic, A.B. Aebbersold, J.A.E. Manson, Effect of interfacial interactions on the electromechanical response of poly(vinylidene fluoride-trifluoroethylene)/ $\text{BaTiO}_3$  composites and its time dependence after poling, *Compos. Sci. Technol.* 114 (2015) 103–109.
- [13] G.K.L. Goh, F.F. Lange, S.M. Haile, C.G. Levi, Hydrothermal synthesis of  $\text{KNbO}_3$  and  $\text{NaNbO}_3$  powders, *J. Mater. Res.* 18 (2003) 338–345.
- [14] K.I. Kakimoto, I. Masuda, H. Ohsato, Lead-free  $\text{KNbO}_3$  piezoceramics synthesized by pressure-less sintering, *J. Eur. Ceram. Soc.* 25 (2005) 2719–2722.
- [15] T. Shiraiishi, N. Kaneko, M. Ishikawa, M. Kurosawa, H. Uchida, H. Funakubo, Ferroelectric and piezoelectric properties of  $\text{KNbO}_3$  films deposited on flexible organic substrate by hydrothermal method, *Jpn. J. Appl. Phys.* 53 (2014).
- [16] D.G. Lim, B.S. Jang, S.I. Moon, C.Y. Won, J. Yi, Characteristics of  $\text{LiNbO}_3$  memory capacitors fabricated using a low thermal budget process, *Solid State Electron.* 45 (2001) 1159–1163.
- [17] W. Weng, H. Wang, N. Ma, Y. Wu, J. Li, Effect of domain structure on the damping properties of  $\text{LiNbO}_3/\text{Al}$  composites, *Mater. Des.* 31 (2010) 4116–4121.
- [18] H. Zhu, Z. Zheng, X. Gao, Y. Huang, Z. Yan, J. Zou, H. Yin, Q. Zou, S.H. Kable, J. Zhao, Y. Xi, W.N. Martens, R.L. Frost, Structural evolution in a hydrothermal reaction between  $\text{Nb}_2\text{O}_5$  and  $\text{NaOH}$  solution: from  $\text{Nb}_2\text{O}_5$  grains to microporous  $\text{Na}_2\text{Nb}_2\text{O}_6 \cdot 2/3 \text{ H}_2\text{O}$  fibers and  $\text{NaNbO}_3$  cubes, *J. Am. Chem. Soc.* 128 (2006) 2373–2384.
- [19] H. Song, W. Ma, Hydrothermal synthesis of submicron  $\text{NaNbO}_3$  powders, *Ceram. Int.* 37 (Apr. 2011) 877–882.
- [20] H.B. Kang, C.S. Han, J.C. Pyun, W.H. Ryu, C.-Y. Kang, Y.S. Cho, ( $\text{Na,K}$ ) $\text{NbO}_3$  nanoparticle-embedded piezoelectric nanofiber composites for flexible nanogenerators, *Compos. Sci. Technol.* 111 (2015) 1–8.
- [21] Y.I. Yuzuyuk, P. Simon, E. Gagarina, L. Hennem, D. Thiaudière, V.I. Torgashev, S.I. Raevskaya, I.P. Raevskii, L.A. Reznitchenko, J.L. Sauvajol, Modulated phases in  $\text{NaNbO}_3$ : Raman scattering, synchrotron x-ray diffraction, and dielectric investigations, *J. Phys. Condens. Matter* 17 (2005) 4977–4990.
- [22] A. Moure, T. Hungria, A. Castro, L. Pardo, Microstructural effects on the phase transitions and the thermal evolution of elastic and piezoelectric properties in highly dense, submicron-structured  $\text{NaNbO}_3$  ceramics, *J. Mater. Sci.* 45 (2009) 1211–1219.
- [23] Y. Yoneda, D. Fu, S. Kohara, Local structure analysis of  $\text{NaNbO}_3$ , *J. Phys. Conf. Ser.* 502 (2014) 012022.
- [24] A. Moure, T. Hungria, A. Castro, L. Pardo, Quantitative microstructural analysis and piezoelectricity of highly dense, submicron-structured  $\text{NaNbO}_3$  ceramics from mechanically activated precursors, *J. Eur. Ceram. Soc.* 29 (2009) 2297–2308.
- [25] H. Ge, Y. Hou, C. Xia, M. Zhu, H. Wang, H. Yan, Preparation and piezoelectricity of  $\text{NaNbO}_3$  high-density ceramics by molten salt synthesis, *J. Am. Ceram. Soc.* 94 (2011) 4329–4334.
- [26] T. Wada, K. Tsuji, T. Saito, Y. Matsuo, Ferroelectric  $\text{NaNbO}_3$  ceramics fabricated by spark plasma sintering, *Jpn. J. Appl. Phys.* 42 (Part 1) (2003) 6110–6114.
- [27] C. David, J.-F. Capsal, L. Laffont, E. Dantras, C. Lacabanne, Piezoelectric properties of polyamide 11/ $\text{NaNbO}_3$  nanowire composites, *J. Phys. D. Appl. Phys.* 45 (2012) 415305.
- [28] H. Pan, G. Zhu, X. Chao, L. Wei, Z. Yang, Properties of  $\text{NaNbO}_3$  powders and ceramics prepared by hydrothermal reaction, *Mater. Chem. Phys.* 126 (2011) 183–187.
- [29] T. Sasuga, M. Hagiwara, Molecular motions of non-crystalline poly(aryl ether-ether-ketone) PEEK and influence of electron beam irradiation, *Polymer* 26 (1985) 501–505.
- [30] L. David, S. Etienne, Molecular mobility in para-substituted polyaryls. 1. Sub-Tg relaxation phenomena in poly(aryl ether ether ketone), *Macromolecules* 25 (1992) 4302–4308.
- [31] E.H. Kerner, The elastic and thermo-elastic properties of composite media, *Proc. Phys. Soc. Sect. B.* 69 (2002) 808–813.
- [32] R.E. Newnham, D.P. Skinner, L.E. Cross, Connectivity and piezoelectric-pyroelectric composites, *Mater. Res. Bull.* 13 (1978) 525–536.
- [33] C. Iurian, F. Ikhouane, J.J. Rodellar Benedé, R. Griñó, Identification of a System With Dry Friction, *Reports Recer. l'Institut d'Organització i Control Sist. Ind.* 1, 2005.
- [34] W. Margaret, Sodium Potassium Niobate Based Piezoelectric Ceramics, University of Manchester, 2012 (dissertation).